INTERNATIONAL JOURNAL FOR NUMERICAL METHODS IN FLUIDS, VOL. 8, 1121–1134 (1988)

A SPECTRAL MULTI-DOMAIN TECHNIQUE FOR VISCOUS COMPRESSIBLE REACTING FLOWS

M. G. MACARAEG AND C. L. STREETT
NASA Langley Research Center, Hampton, VA 23665, U.S.A.

SUMMARY

The first application of a spectral multi-domain method for viscous compressible flow is presented. The method imposes a global flux balance condition at the interface so that high-order continuity of the solution is preserved. The global flux balance is imposed in terms of a spectral integral of the discrete equations across adjoining domains. Since the discretized equations interior to each domain are solved uncoupled from each other and since the interface relation has a block structure, the solution scheme can be adapted to the particular requirement in each subdomain. To illustrate these advantages a Mach 11 shock calculation is presented to study the chemical kinetics initiated as air passes through a fully resolved shock wave.

KEY WORDS Spectral multi-domain method Viscous compressible flow Shock waves Chemical kinetics

INTRODUCTION

A number of spectral domain decomposition techniques have appeared in the literature and are becoming accepted tools for fluid dynamical calculations. For example, the spectral element method which applies finite element methodology using Galerkin spectral discretization in the variational formulation within elements is a popular technique.[1, 2] This technique utilizes a split Galerkin–collocation discretization which restricts its application to convection–diffusion problems for incompressible flows. The spectral element method in practice is used in a manner similar to classical finite element techniques: low-order internal discretization using many elements with no internal stretchings to improve resolution. The technique is most easily implemented if each element utilizes the same number of collocation points. Other domain decomposition techniques involve explicit enforcement of C^1 continuity across the interface.[3, 4] It is not clear how well these techniques perform for strongly convection-dominated problems; the second author's experience with such techniques[5] has shown them to be not entirely satisfactory.

The spectral multi-domain technique of the present paper was developed with compressible flow applications in mind. The multiple scales associated with chemically reacting flows and transition, both features of hypersonic aerodynamics, were a further consideration in developing the multi-domain technique. The former issue will be addressed by incorporating a non-equilibrium chemistry model for air into the spectral multi-domain Navier–Stokes solution method. The application will focus on the chemical kinetics initiated as air passes through a fully resolved shock wave.

Received 19May 1987
Revised 14 October 1987

SPECTRAL MULTI-DOMAIN TECHNIQUE

Spectral collocation methods have proven to be an efficient discretization scheme for many aerodynamic (e.g. References 5–9) and fluid mechanic (e.g. References 10–13) problems. The higher-order accuracy and resolution shown by these methods allows one to obtain engineering-accuracy solutions on coarse meshes, or alternatively to obtain solutions with very small error. However, there exist drawbacks to spectral techniques which prevent their widespread usage. One drawback has been the requirement that a complicated physical domain must map onto a simple computational domain for discretization. This mapping must be smooth if the high-order accuracy and exponential convergence rates associated with spectral methods are to be preserved.[6] Additionally, even smooth stretching transformations can decrease the accuracy of a spectral method if the stretching is severe.[9] Such stretchings would be required to resolve the thin viscous region in an external aerodynamic problem or the widely disparate scales which occur in chemically reacting flows. Furthermore, problems with discontinuities in boundary conditions, very high-gradient regions or shocks cause oscillations in the spectral solution. The above situations are more the rule than the exception in hypersonic flows.

These restrictions are overcome in the present method by splitting the domain into regions, each of which preserves the advantages of spectral collocation and allows the ratio of the mesh spacings between regions to be several orders of magnitude higher than allowable in a single domain.[14] Adjoining regions are interfaced by enforcing a global flux balance which preserves high-order continuity of the solution. This interface technique maintains spectral accuracy, even when mappings and/or domain sizes are radically different across the interface, provided that the discretization in each individual subdomain adequately resolves the solution there.

Spectral flux balance interface technique

A simple one-dimensional, two-region example will serve to illustrate the present method for interfacing two collocation-discretized regions. Given the second-order, potentially non-linear boundary value problem

$$\begin{aligned} &[F(U)]_x - \nu U_{xx} = S(U), \quad x \in [-1, 1], \\ &U(-1) = a, \qquad U(1) = b, \end{aligned} \tag{1}$$

we wish to place an interface at the point $x = m$ and have independent collocation discretization in the regions $x^{(1)} \in [-1, m]$ and $x^{(2)} \in [m, 1]$. Even though the point $x = m$ is an interior point to the problem domain, simply applying a collocation statement there, utilizing a combination of the discretizations on either side, will not work; the resulting algebraic system is singular. This is because the spectral second-derivative operator has two zero eigenvalues; thus the patching together of two spectrally discretized domains yields potentially four zero eigenvalues in the overall algebraic system. Two of these eigenvalues are accounted for by imposition of boundary conditions and one by continuity of the solution at the interface, leaving one zero eigenvalue in the system. To alleviate this difficulty, a global statement of flux balance is used. Rewriting (1) as

$$[G(U)]_x = S(U), \tag{2}$$

where the flux is

$$G(U) = F(U) - \nu U_x, \tag{3}$$

then integrating (2) from -1 to 1 results in

$$G(U)|_{x=1} - G(U)|_{x=-1} + [G]|_{x=m} = \int_{-1}^{1} S(U)\mathrm{d}x. \tag{4}$$

If the jump in flux at the interface, $[G]$, is zero, then (4) may be written

$$G(U)|_{x=-1} + \int_{-1}^{m} S(U)\mathrm{d}x = G(U)|_{x=1} - \int_{m}^{1} (U)\mathrm{d}x. \tag{5}$$

The statement of global flux balance across the two regions, along with the assumption that the solution is continuous, provides the condition necessary to close the equation set which results from spectral discretization of (1) in two regions. Note that the left side of (5) involves the discretization in the region $x^{(1)} \in [-1, m]$ while the right side involves the region $x^{(2)} \in [m, 1]$. Since spectral collocation discretization strongly couples all points in their respective regions, (5) couples all points in both discretizations.

Note also that no statement is made concerning whether or not (1) is advection- or diffusion-dominated. Equation (1) is considered a scalar equation here, although the above is extendable to a system.

Examples

In this section the present global flux balance, spectral multi-domain method will be shown as applied to a number of one- and two-dimensional test problems. The one-dimensional examples will serve to show that this method can maintain the exponential-order error convergence which is characteristic of collocation methods, even when adjoining domains have radically different discretizations in terms of domain size, number of points or stretching. Two-dimensional examples will demonstrate the ability of the multi-domain technique to deal with discontinuous boundary conditions and coefficients; a calculation on a non-orthogonal mesh will also be given to show the generality of the method.

The first example will illustrate the capability of the method for resolving very high gradients in a solution while imposing an interface condition which preserves spectral accuracy. Consider the Burgers' equation

$$\begin{aligned} &U_t + \tfrac{1}{2}(\mathrm{U}^2)_x = \nu U_{xx}, \quad x \in [-1, 1], \\ &U(-1, t) = U(1, t) = 0, \qquad U(x, 0) = -\sin(\pi x). \end{aligned} \tag{6}$$

This problem has been studied extensively by a number of authors, using techniques ranging from standard finite difference to single-domain spectral collocation and spectral element.[15] The solution to this problem develops a very steep gradient region in the centre of the domain; the slope at $x = 0$ reaches a maximum, then decreases as the initial energy is dissipated away. For the parameters studied in Reference 15 ($\nu = 0{\cdot}01/\pi$), this maximum is reached at $t \simeq 0{\cdot}5$; a very accurate analytical solution gives a value of 152·00516 for the maximum slope. The evolution of this solution calculated from the present method is shown in Figure 1 at time increments of 0·1.

In the present study of this problem three domains were used, the middle domain spanning a very small region ($\pm 0{\cdot}05$) around the 'shock'. Additionally, a mapping was applied in the middle domain to improve resolution, of the form

$$x^{\mathrm{T}} = \sinh(\beta x^{\mathrm{C}})/\sinh(\beta), \tag{7}$$

where both the computational coordinate x^{C} and the transformed co-ordinate x^{T} are $\in [-1, 1]$ and β is an $O(1)$ constant chosen to control the packing at $x^{\mathrm{T}} = 0$. The maximum stretching

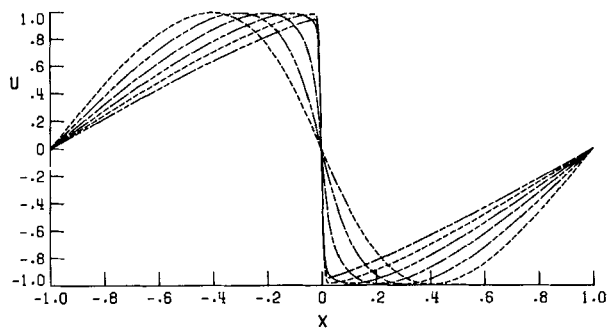

Figure 1. Computed solution to equation (6) at time increments of 0·1; $\nu = 0{\cdot}01/\pi$, discretization 32/33/32, interfaces at $\pm 0{\cdot}05$

allowable in this mapping is subject to the same restriction as stretchings in single-domain discretizations, e.g. maximum metric ratios of the order of 10^3.

A second-order backward-Euler time-stepping technique was used; a time-step refinement study was performed to extrapolate out time-stepping errors. For this small one-dimensional problem, the algebraic system resulting from the spectral discretization of the equation plus interface conditions was Newton-linearized and solved directly using Gaussian elimination at each time step.

From the comparison study contained in Reference 15, the two methods giving the best accuracy for a given number of grid points were single-domain spectral collocation and spectral element. The collocation scheme used a mesh stretching with a maximum-to-minimum metric ratio of about 100. Beyond this stretching a degradation in accuracy was found to occur. The spectral element discretization utilized four elements with 16 nodes in each. The behaviour of the error in maximum slope from these methods and the present scheme is shown in Table I. As can be seen, the present method with just 35 total points (12 points in the outer domain, 13 points in the middle domain, 12 points in the left outer domain (hereafter denoted 12/13/12)) yields results of equivalent accuracy to the spectral element and single-domain spectral collocation methods of Reference 15 which both use 64 total points. Further mesh refinements using the present method show exponential-order error convergence, as seen in Table I by the order-of-magnitude decrease in relative error as the mesh is refined to 20/21/20, and again with mesh refinement to 32/33/32. For the same total number of points, the present method is an order of magnitude more accurate than the single-domain collocation or spectral element solutions of Reference 15.

In order to demonstrate the capability of the present method to handle radically different mappings between adjacent domains, a solution to the above Burgers' equation for $\nu = 10^{-4}$ is shown in Figure 2. The maximum slope for this solution is greater than 5000. The discretization used was 12/31/12; the stretching in the middle domain was so severe that the ratio of the largest mesh spacing in the outer domains to the smallest in the middle domain is greater than 10^5. A factor-of-5000 magnification of the high-gradient region of this solution is shown in Figure 3. The emphasis in this plot is the oscillation-free resolution of this region. (Linear interpolation between points in used for plotting, making the plot appear somewhat jagged).

To demonstrate the maintenance of conservation by the present interface technique, an initial condition was applied to the Burgers' equation to generate a moving 'shock' which passed through the interface, as shown in Figure 4. No oscillations, reflections or abrupt changes in wave speed are seen as the 'shock' passes through the interface. A very skewed discretization of 12/17/27 was used for this case. Note that a multi-domain method formulated only for hyperbolic

Table I. Maximum slope and percentage relative error in maximum slope for Burgers' equation (6); comparison of present method with results from Reference 15

Method	Discretization	Maximum slope	% relative error
	3 domains:		
Present	12/13/12	152·03544	1·99 (−2)
Present	20/21/20	152·00011	3.23 (−3)
Present	31/33/32	152·00513	2·14 (−4)
Spectral element[15]	4 elements 16/16/16/16	152·04	2·29 (−2)
Spectral collocation[15]	1 domain: 64	152·025	1·31 (−2)
Exact[15]		152·00516	

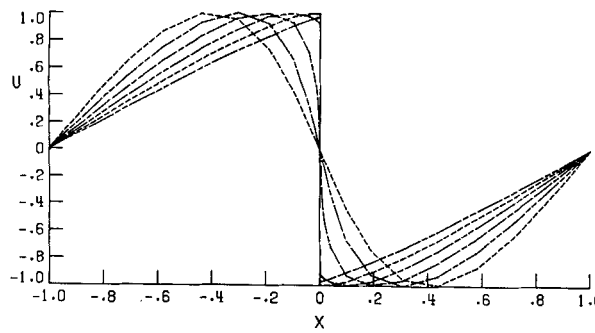

Figure 2. Computed solution to equation (6) at time increments of 0·1; $\nu = 10^{-4}$, discretization 12/31/12, interfaces at $\pm 0{\cdot}02$

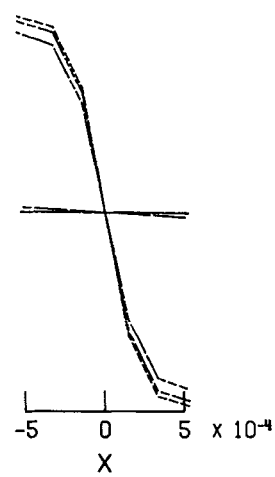

Figure 3. Expansion of high-gradient region of Figure 2

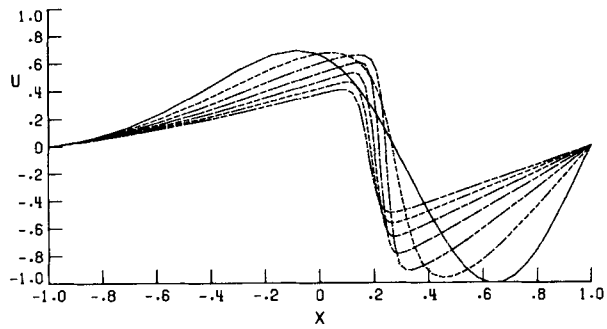

Figure 4. Computed solution to Burgers' equation with moving shock; $\nu = 0{\cdot}01$, discretization 12/17/27, interfaces at $\pm 0{\cdot}25$

or elliptic equations would be unable to perform well on this problem, since the dissipation-dominated region passes through the interface.

Spectral discretization of problems with discontinuous coefficients or source terms (or equivalently, discontinuous transformation metrics) or discontinuities in boundary conditions typically yields solutions with large oscillations and low-order error convergence. The present multi-domain technique may be used to isolate such discontinuities and recover exponential-order convergence. Figure 5 illustrates such an application; solutions to Laplace's equation are shown in which a jump in boundary conditions is enforced on one side of the domain. When the discontinuity lies at a point interior to one of the discretizations (right boundary of Figure 5), oscillations are seen clearly in the solution isolines. When the discontinuity occurs where the interface meets the boundary, however, the contour lines are smooth (upper boundary of Figure 5).

Another example of the application of the multi-domain technique to isolate a discontinuity is in the solution of the following equation:

$$\begin{aligned} &\nabla\cdot(k\nabla U) = 0, \quad x \in [-2, 2], \quad y \in [-1, 1], \\ &U(x, -1) = U(x, 1) = U(-2, y) = 0, \qquad U(2, y) = \cos(\tfrac{1}{2}\pi y), \end{aligned} \tag{8}$$

where $k = k_1$, $-2 \leqslant x \leqslant 0$, and $k = k_2 = 10k_1$, $0 < x \leqslant 2$, with the interface at the line of coefficient discontinuity as shown in Figure 6. The computed solution is everywhere smooth and the gradient jump at $x = 0$ is automatically enforced.

To demonstrate the generality of the technique, a Poisson equation is solved on the skewed two-domain mesh shown in Figure 7.[16] This mesh, containing 17×16 and 18×17 points in the left and right domains respectively, is generated by first choosing the interface line, in this case a cubic polynomial. Chebyshev distributions with respect to arc length are used to establish the mesh points on the interface, as well as along the domain boundaries at $x = \pm 2$. One curvilinear co-ordinate family is generated by connecting these corresponding points with straight lines. Mesh points along these co-ordinate lines are then established with Chebyshev distributions with respect to arc length, resulting in a sheared non-orthogonal mesh. The governing equation is written in generalized contravariant flux form; the metrics are evaluated by spectral differentiation of the co-ordinate distributions. The flux component normal to the interface is taken to be continuous in the interface condition. As can be seen in the isolines of the solution shown in Figure 8, the solution is everywhere smooth and regular.

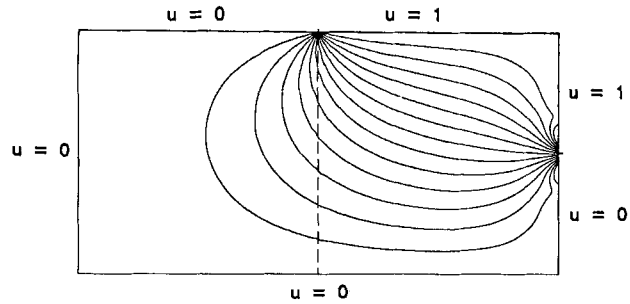

Figure 5. Computed solution to Laplace's equation with discontinuous boundary conditions as noted; interface at broken line

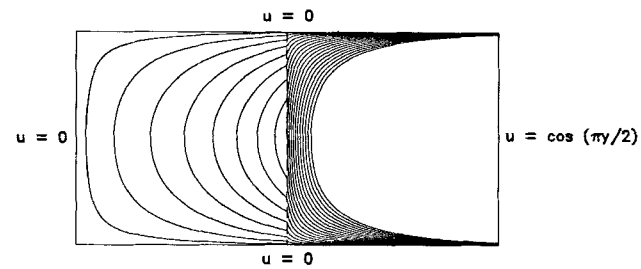

Figure 6. Computed solution to equation (8); interface at broken line

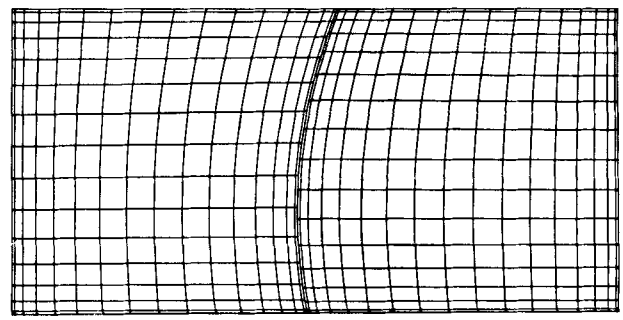

Figure 7. Skewed two-domain mesh

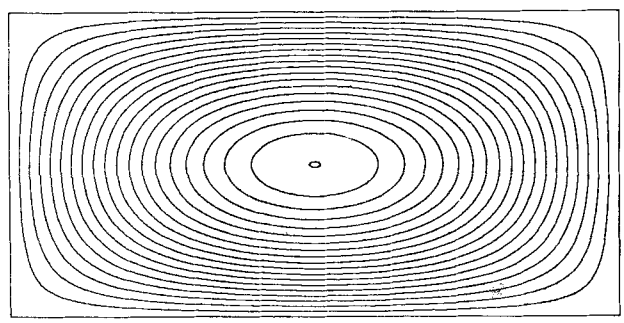

Figure 8. Solution of Poisson equation on mesh shown in Figure 7

NUMERICAL MODEL OF NON-EQUILIBRIUM SHOCK FLOW

The above technique will model the chemical kinetics and flow kinematics of a non-ionized air mixture (O_2, N_2, NO, O and N) passing through a fully resolved shock wave, thus alleviating the need for artificial viscosity. The governing equations are the quasi-one-dimensional Navier–Stokes equations[17] and the species conservation equation.[18] The quasi-one-dimensional form is used to provide an artifice for controlling the shock location in the physical space for this otherwise indeterminate problem.

The conservation equations can be written as

$$\frac{\partial \mathbf{U}}{\partial t}+\frac{\partial \mathbf{F}}{\partial x}=\frac{\partial \mathbf{V}}{\partial x}+\mathbf{W} \tag{9}$$

where the dependent variables are denoted by **U**, the convective flux by **F**, the dissipative flux by **V** and the production rate by **W**. The equations are non-dimensionalized by dividing the state and transport parameters by their dimensional free-stream values. Each of the quantities **U**, **F**, **V** and **W** has eight components. These expressions are given explicitly in the Appendix.

The viscosity of each of the individual species is calculated from a curve-fit relation.[19] Similarly, curve fits are used to obtain specific heats, internal energies and enthalpies.[20, 21] The thermal conductivity of each species is calculated from the Euken semi-empirical formula using the viscosity and specific heat of the species. Appropriate mixture rules are next used to obtain the transport properties of the mixture.[22] Experimental values of bulk viscosities, as obtained from acoustical interferometry and related experiments, are taken from Truesdell.[23]

In the present work the diffusion model is limited to binary diffusion, with the binary diffusion coefficients specified by the Lewis number. The value of the Lewis number used is 1·4.

The temperature range under study will not exceed 8000 K for conditions at an altitude of approximately 190000 ft. Therefore ionization reactions, which occur at roughly 9000 K, are not included. The chemical reactions utilized for the non-ionized air mixture are impact dissociation and exchange reactions. The 17 reactions included in the present study can be found in Reference 18, which also lists ionization reactions and gives the constants needed to evaluate reaction rates.

Initial conditions are obtained from a spectral multi-domain code for solution of the Navier–Stokes equations with equilibrium chemistry, written for the above problem. These governing equations may be found in Reference 17. Transport properties are obtained in the manner previously discussed. The routines of Reference 20 generalized for air are used to obtain equilibrium concentrations.

NUMERICAL ALGORITHM

The multi-domain discretization involves three independent subdomains, with the shock located in the centre subdomain. Shock jump conditions are obtained by an iterative procedure to solve the Rankine–Hugoniot relations for real air.

A direct inversion of the coupled system is utilized to obtain a fully implicit method. The conserved variables are written in delta form, and a pseudo-time iteration using backward Euler is utilized to obtain the steady-state solution as follows. Time-local linearization of equation (19) leads to the implicit form of the equation over the time step Δt:

$$\left\{\mathbf{I}+\left[\Delta t\frac{\partial}{\partial x}\left(\mathbf{A}+\frac{\partial \mathbf{B}}{\partial x}\right)-\frac{\partial^2}{\partial x^2}\mathbf{B}-\mathbf{S}\right]\right\}\Delta U=\Delta t\left(\mathbf{W}+\frac{\partial}{\partial x}(-\mathbf{F}+\mathbf{V})\right), \tag{10}$$

where **I** is the unit matrix and **A**, **B** and **S** are Jacobian matrices; $\mathbf{A}=\partial(\mathbf{F}-\mathbf{V})/\partial U$, $\mathbf{B}=\partial(\mathbf{F}-\mathbf{V})/\partial U_x$ and $\mathbf{S}=\partial\mathbf{W}/\partial U$. These Jacobians are obtained analytically and are evaluated at the previous time step. Because of the large rank and ill condition of the Jacobian matrix, iterative improvement of the Gaussian elimination solution was found to be required. Nonetheless, the scheme required less than one second per time step on the Cray-2 at NASA Ames for typical discretizations used in this study.

METHOD VERIFICATION

The validity of the multi-domain Navier–Stokes algorithm is demonstrated by comparison with experiment. A low-density wind tunnel study of shock-wave structure and relaxation phenomena in gases was conducted by Sherman.[24] The experiment measured shock-wave profiles recorded in terms of the variation in the equilibrium temperature of a small-diameter wire oriented parallel to the plane of the shock, as the wire was moved through the shock zone. The free stream Mach number was 1·98. For this test case, a Navier–Stokes spectral multi-domain calculation is performed for a perfect gas with temperature-dependent properties and a non-zero bulk viscosity corresponding to air.[23] A comparison with experimental temperatures normalized by the free-stream temperature versus normalized distance is given in Figure 9. The experimental data points are represented by the open circles. The numerical results fall within a symbol width of the data. The multi-domain technique utilizes three domains. The centre domain, located between $x=-0{\cdot}15$ and $x=0{\cdot}3$, contains 21 points; the outer domains contain 11 points each. The computational domain spans -1 to 1. The unit Reynolds number of the flow is 80. A calculation for a unit Reynolds number of 1000 is given in Figure 10, which shows the ability of the method to accurately resolve strong gradients without numerical oscillations. The plot is of Mach number versus normalized distance. Three domains are again used; the centre domain contains 17 points and the outer domains contain 11 points each, with the interfaces located at $-0{\cdot}15$ and $-0{\cdot}1$.

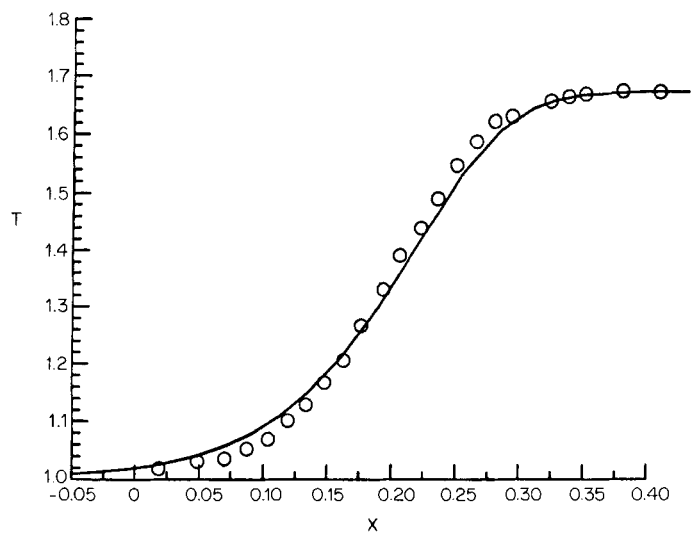

Figure 9. Comparison of multi-domain Navier–Stokes calculation with experimentally obtained temperatures; $M_\infty=1{\cdot}98$, $Re=80$, discretization 11/21/11, interfaces at $-0{\cdot}15$ and 0·3

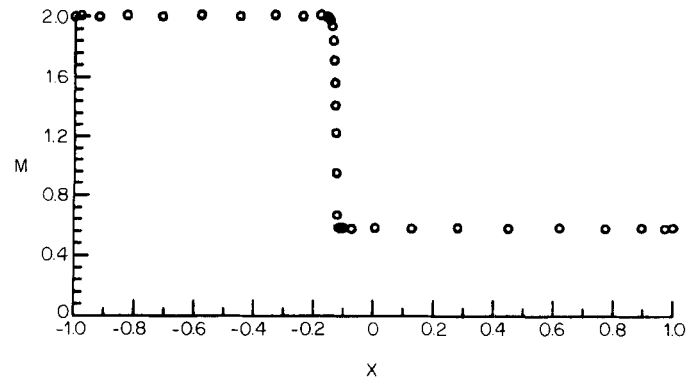

Figure 10. Computed solution for $Re = 1000$; discretization 11/17/11, interfaces at $-0{\cdot}15$ and $-0{\cdot}1$

RESULTS

The method is used to calculate the chemical kinetics initiated as air passes through a hypersonic shock wave. The case to be discussed with respect to the effects of non-equilibrium assumptions on the conditions is $M_\infty = 11{\cdot}0$, $T_\infty = 350$ K and $\rho_\infty = 6 \times 10^{-8}$ g cm^{-3}. These conditions invoke primarily O_2 dissociations, with N_2 dissociations just beginning. Temperatures are not yet high enough for ionization to occur, so electronic energy modes remain unexcited. A fundamental study of the effects which artificial viscosity used in large-scale calculations has on the chemical kinetics occurring in the near-shock regime is given in Reference 25.

Typical discretizations used in this study were 15, 27 and 33 points in the upstream, middle and downstream domains respectively. The backward-Euler implicit time-stepping algorithm typically required less than 2000 iterations to converge from an equilibrium starting solution, with a reduction of at least eight orders of magnitude in maximum residual.

It is interesting to note the effect of downstream boundary conditions of the chemical species on the numerical results. Two boundary conditions are compared in Figure 11. The first involves imposing the equilibrium end state concentrations corresponding to the post-shock temperature and density values from the equilibrium jump conditions. The second involves a zero-gradient boundary condition on the species' concentrations. The plot is of the log of the concentration in the relaxation zone versus normalized distance behind the shock. It is evident that the extrapolation condition leads to a smooth profile of concentrations down to a desired end state, whereas an imposed equilibrium end state causes oscillations in the numerics and a resulting discontinuity between the imposed equilibrium end state and the pathway chosen by the chemical kinetics calculation.

To test the effect of the extrapolation boundary conditions on the chemical kinetics, a comparison is made between a computation for which the post-shock physical domain is long enough to allow the concentrations to relax to their final values, and one in which the domain is severely truncated. The results for $[O_2]$ and [O] are shown in Figure 12, with the truncated-domain ($[-1, 1]$) solution represented by symbols and the extended-domain ($[-1, 120]$) solution shown as curves. As can be seen, the profiles are identical.

Figure 13 shows the Mach number and temperature profiles for the resolved shock. Note that only the near-shock region on a greatly expanded scale is plotted in the figure. The endpoints are at -1 and 200 and the interface points at $-0{\cdot}3$ and $0{\cdot}1$. The temperature overshoot is produced by the conversion of kinetic energy to thermal energy, on a scale too small for the chemistry to

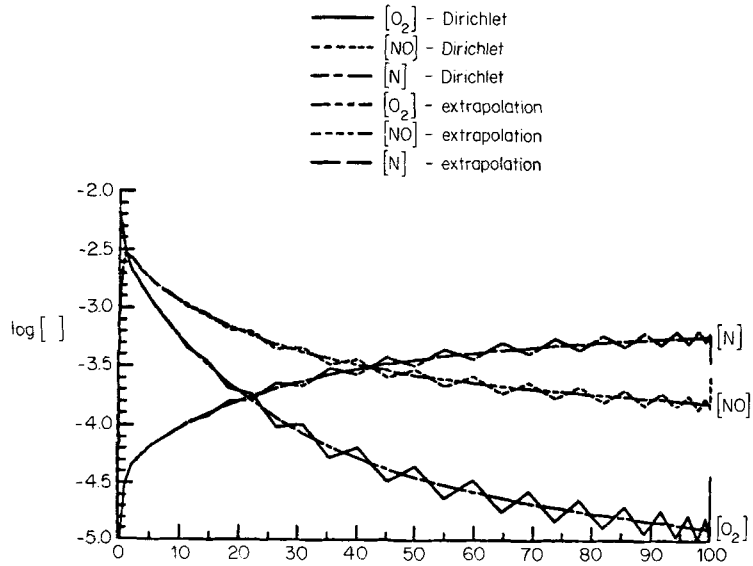

Figure 11. Species concentrations in the relaxation zone for both Dirichlet (imposed equilibrium end state) and extrapolation boundary conditions

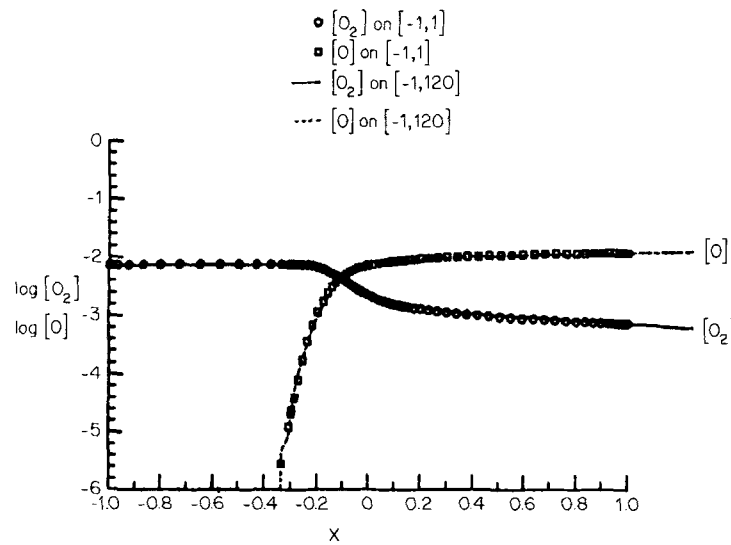

Figure 12. Comparison of $[O_2]$ and [O] in the relaxation zone spanning $[-1, 1]$ and $[-1, 120]$

respond. Thus the near-shock chemistry is essentially frozen, and the ratio of enthalpy to internal energy remains near its free-stream value. The chemical reactions then begin to respond on their own scale, as dictated by the reaction rate constants used in the model. A fraction of this thermal energy is absorbed by the reactions, thus lowering the temperature. Figure 14 shows the profiles for [N] and [NO] in the relaxation zone.

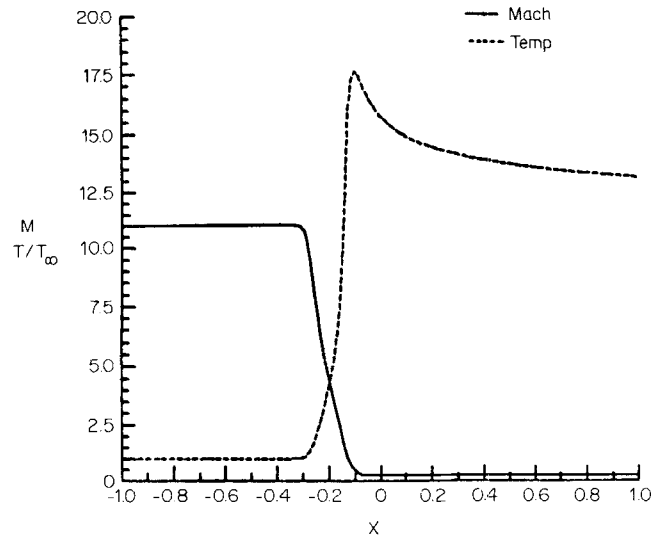

Figure 13. Mach number and temperature profiles for compressible viscous calculation ($M_\infty = 11$); computational domain $[-1, 200]$, interfaces at $-0{\cdot}3$ and $0{\cdot}1$, discretization 15/27/33

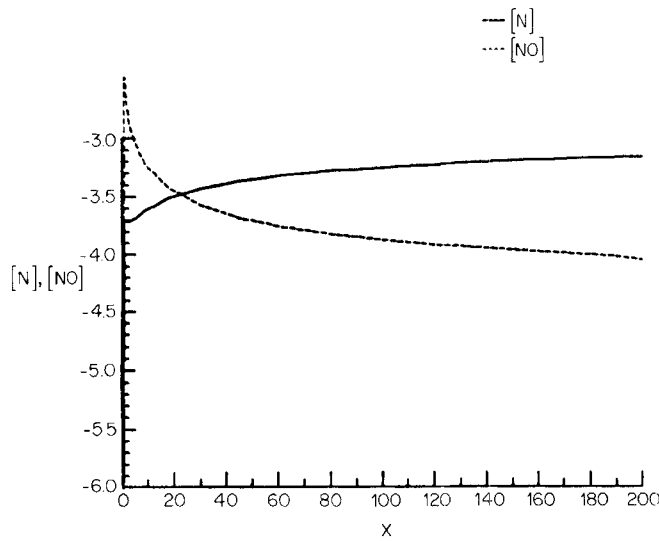

Figure 14. Shock-initiated chemical kinetics ($M_\infty = 11$); discretization 15/27/33, interfaces at $-0{\cdot}3$ and $0{\cdot}1$

CONCLUSIONS

The present global flux balance, spectral multi-domain method has demonstrated maintenance of exponential-order accuracy on a variety of advection- and diffusion-dominated test problems. Extremely large differences in discretization across an interface, as a result of domain size, number of points and stretchings, have been shown not to disrupt this property of the present method. Additionally, this technique can be used to isolate certain types of coefficient, mapping or boundary condition discontinuities.

These advantages have made possible the first compressible Navier–Stokes calculation by a spectral multi-domain technique. In addition, a Mach 11 shock calculation with non-equilibrium chemistry was performed to study the chemical kinetics initiated as air passes through a fully resolved shock wave.

APPENDIX

Non-equilibrium one-dimensional Navier–Stokes equations

$$\frac{\partial \mathbf{U}}{\partial t}+\frac{\partial \mathbf{F}}{\partial x}=\frac{\partial \mathbf{V}}{\partial x}+\mathbf{W}$$

Conservation variables

$U_i=\rho\gamma_i, \quad 1\leqslant i\leqslant \mathrm{NS}$ (number of species)

$U_{\mathrm{NS}+1}=\rho$

$U_{\mathrm{NS}+2}=\rho u$

$U_{\mathrm{NS}+3}=\rho E$

Convective fluxes

$F_i=uU_i, \quad 1\leqslant i\leqslant \mathrm{NS}$

$F_{\mathrm{NS}+1}=\rho u$

$F_{\mathrm{NS}+2}=\rho u^2+P$

$F_{\mathrm{NS}+3}=(E+P)u$

Viscous fluxes

$$V_i=\frac{Le}{Pr\ Re}\mu\frac{\partial \gamma_i}{\partial x}, \quad 1\leqslant i\leqslant \mathrm{NS}$$

$$V_{\mathrm{NS}+1}=0$$

$$V_{\mathrm{NS}+2}=\frac{\lambda+2\mu}{Re}\frac{\partial \rho u}{\partial x}$$

$$V_{\mathrm{NS}+3}=\frac{\lambda+2\mu}{Re}u\frac{\partial \rho u}{\partial x}+\frac{\beta k}{(\beta-1)Pr\ Re}\frac{\partial}{\partial x}\left[(\beta-1)\left(E-\frac{u^2}{2}\right)\right]\Big/ z+\frac{1-\beta}{z}\frac{Le\, m_\infty}{Pr\ Re}\left(E-\frac{\rho u^2}{2}\right)\sum_{i=1}^{\mathrm{NS}}h_i\frac{\partial \gamma_i}{\partial x}$$

where m_∞ is the free-stream molecular weight, Le is the Lewis number, z is the compressibility ($P=z\rho T$), h_i is the enthalpy of species i and $\beta=h/e$.

Source production terms

$$W_i=\sum_{r=1}^{\mathrm{NR}}(\beta_{i,r}-\alpha_{i,r})(R_r^f-R_r^b)$$

$$R_r^f=k_r^f\prod_{j=1}^{\mathrm{NS}}(\rho\gamma_j)^{\alpha_{j,r}} \qquad R_r^b=k_r^b\prod_{j=1}^{\mathrm{NS}}(\rho\gamma_j)^{\beta_{j,r}}$$

$$k_r^f=A_1T^{A_2}\exp(-A_3/T) \qquad k_r^b=B_1T^{B_2}\exp(-B_3/T)$$

where NR is the number of reactions, $\alpha_{i,r}$ and $\beta_{i,r}$ are the stoichiometric coefficients for forward and backward reactions respectively and $W_{NS+1} = W_{NS+2} = W_{NS+3} = 0$.

REFERENCES

1. A. T. Patera, 'A spectral element method for fluid dynamics: laminar flow in a channel expansion', *J. Comput. Phys.* **54,** 468–488 (1984).
2. N. Ghaddar, A. T. Patera and B. Mikic, 'Heat transfer enhancement in oscillatory flow in a grooved channel', *AIAA Paper 84-0495*, 1984.
3. B. Metivet and Y. Morchoisne, 'Multi-domain spectral techniques for viscous flow calculations', in *Proc. 4th Conf. on Numerical Methods in Fluid Dynamics*, October 1981.
4. H. H. Migliore and E. G. McReynolds, 'Multi-element collocation solution for convective dominated transport', in C. Taylor, J. Johnson and W. Smith (eds), *Numerical Methods in Laminar and Turbulent Flow*, 1983.
5. D. L. Gottlieb, L. Lustman and C. L. Streett, 'Spectral methods for two-dimensional shocks', *ICASE Report No. 82-83*, November 1982.
6. C. L. Streett, 'A spectral method for the solution of transonic potential flow about an arbitrary two-dimensional airfoil', *AIAA Paper 83-1949-CP*, presented at *AIAA 16th Computational Fluid Dynamics Conf.*, Danvers, MA, 13–15 July 1983.
7. M. Y. Hussaini, C. L. Streett and T. Zang, 'Spectral methods for partial differential equations', *NASA CR-172248*, August 1983.
8. C. L. Streett, T. A. Zang and M. Hussaini, 'Spectral multigrid methods with applications to transonic potential flow', *Comput. Phys.*, **56,** 43–76 (1984).
9. C. L. Streett, T. A. Zang and M. Y. Hussaini, 'Spectral methods for solution of the boundary-layer equation', *AIAA Paper 84-0170*, presented at *AIAA 22nd Aerospace Sciences Meeting*, Reno, NV, 9–12 January 1984.
10. M. G. Macaraeg, 'Numerical model of the axisymmetric flow in a heated, rotating spherical shell', *Ph.D. Dissertation*, University of Tennessee Space Institute, TX 1-541-627, June 1984.
11. M. G. Macaraeg, 'The effect of power law body forces on a thermally-driven fluid between concentric rotating spheres', *J. Atmos. Sci.*, **62** (2), 302–304 (1986).
12. M. G. Macaraeg, 'A mixed pseudospectral/finite difference method for the axisymmetric flow in a heated, rotating spherical shell', *J. Comput. Phys.*, **43** (3), 297–320 (1986).
13. M. G. Macaraeg, 'A mixed pseudospectral/finite difference method for a thermally-driven fluid in a nonuniform gravitational field', *AIAA Paper 85-1662*, presented at *AIAA 18th Fluid Dynamics and Plasmadynamics and Laser Conf.*, Cincinnati, OH, 15–18 July 1985, pp. 1483–1487.
14. M. G. Macaraeg and C. L. Streett, 'Improvements in spectral collocation discretization through a multiple domain technique', *Appl. Numer. Math.*, **2** (2), 95–108 (1986).
15. C. Basdevant, M. Deville, P. Haldenwang, J. Lacroix, D. Orland, J. Quazzani, A. Patera and R. Peyret, 'Spectral and finite difference solutions of the Burgers' equation', *Comput. Fluids*, **14,** 23–41 (1986).
16. M. G. Macaraeg and C. L. Streett, 'A spectral multi-domain technique with application to generalized curvilinear coordinates', *Paper No. 14*, presented at *Sixth Int. Symp. on Finite Element Methods in Flow Problems*, 1986.
17. W. C. Davy, C. K. Lombard and M. J. Green, 'Forebody and base real-gas flow in severe planetary entry by a factored implicit numerical method', *AIAA Paper 81-0282*, 1981.
18. C. Park, 'On convergence of computation of chemically reacting flows', *AIAA Paper 85-0247*, 1985.
19. F. G. Blottner, 'Nonequilibrium laminar boundary layer flow of ionized air', *General Electric Report R645D56*, 1964.
20. W. D. Erickson and R. K. Prabhu, 'Rapid combustion of chemical equilibrium composition: an application to hydrocarbon combustion', *AIChE J.* **32,** 1079–1087 (1986).
21. *Janaf Tables, Thermochemical Data*, Dow Chemical Co., 1977.
22. R. B. Bird, W. E. Stewart and E. N. Lightfoot, *Transport Phenomena*, 1966, pp. 554–591.
23. C. Truesdell, 'Precise theory of the absorption and dispersion of forces plan infinitesimal waves according to the Navier–Stokes equations', *J. Rational Mech. Anal.*, **2** (4), 644–721 (1953).
24. F. S. Sherman, 'A low density wind-tunnel study of shock wave structure and relaxation phenomena in gases', *NACA TN-3298*, 1955.
25. M. G. Macaraeg, C. L. Streett and M. Y. Hussaini, 'The effects of artificial viscosity of chemically reacting flows', *ICASE Report No. 87-35*, 1987.